Characterizing the mechanics of cultured cell monolayers

Andrew R. Harris[a,b,c], Loic Peter[a,d], Julien Bellis[e], Buzz Baum[e,f], Alexandre J. Kabla[g], and Guillaume T. Charras[a,f,1]

[a]London Centre for Nanotechnology, University College London, London WC1H 0AH, United Kingdom; [b]Department of Physics, University College London, London WC1E 6BT, United Kingdom; [c]Engineering Doctorate Program, Department of Chemistry, University College London, London WC1H 0AJ, United Kingdom; [d]Ecole Centrale Paris, Grande Voie des Vignes, 92295 Châtenay-Malabry, France; [e]Medical Research Council Laboratory for Molecular Cell Biology, University College London, London WC1E 6BT, United Kingdom; [f]Department of Cell and Developmental Biology, University College London, London WC1E 6BT, United Kingdom; and [g]Engineering Department, University of Cambridge, Cambridge CB2 1PZ, United Kingdom

Edited by David A. Weitz, Harvard University, Cambridge, MA, and approved August 22, 2012 (received for review August 1, 2012)

One-cell-thick monolayers are the simplest tissues in multicellular organisms, yet they fulfill critical roles in development and normal physiology. In early development, embryonic morphogenesis results largely from monolayer rearrangement and deformation due to internally generated forces. Later, monolayers act as physical barriers separating the internal environment from the exterior and must withstand externally applied forces. Though resisting and generating mechanical forces is an essential part of monolayer function, simple experimental methods to characterize monolayer mechanical properties are lacking. Here, we describe a system for tensile testing of freely suspended cultured monolayers that enables the examination of their mechanical behavior at multi-, uni-, and subcellular scales. Using this system, we provide measurements of monolayer elasticity and show that this is two orders of magnitude larger than the elasticity of their isolated cellular components. Monolayers could withstand more than a doubling in length before failing through rupture of intercellular junctions. Measurement of stress at fracture enabled a first estimation of the average force needed to separate cells within truly mature monolayers, approximately ninefold larger than measured in pairs of isolated cells. As in single cells, monolayer mechanical properties were strongly dependent on the integrity of the actin cytoskeleton, myosin, and intercellular adhesions interfacing adjacent cells. High magnification imaging revealed that keratin filaments became progressively stretched during extension, suggesting they participate in monolayer mechanics. This multiscale study of monolayer response to deformation enabled by our device provides the first quantitative investigation of the link between monolayer biology and mechanics.

cell mechanics | tissue mechanics | intermediate filaments

Many of the cavities and free surfaces of the human body are lined by a layer of cells one cell thick. Cells within these monolayers are tightly connected to one another by intercellular junctions. Tight junctions form barriers restricting the passage of solutes while others, such as adherens junctions and desmosomes, integrate the cytoskeletons of constituent cells into a mechanical syncitium. Exposure to mechanical stresses is a normal part of physiology for monolayers: intestinal epithelia are stretched during peristaltic movements in the gut, lung alveoli deform during breathing, and endothelia are exposed to pulsatile fluid shear stresses in blood flow (1–3). The mechanical function of monolayers is particularly apparent in disease where mutations or pathogens affecting the cytoskeleton, adherens junctions, or desmosomes result in increased fragility of tissues (4). Development offers perhaps the most vivid illustration of the role of epithelia in withstanding and exerting mechanical stresses. Indeed, embryonic epithelial tissues are under a constant tension generated by spatially restricted cellular actomyosin contractions (5). When cadherin intercellular adhesion is disrupted, embryos fail to properly develop, displaying a disaggregated ectoderm consistent with mechanical failure (6). Early in vertebrate development, the absence of an extracellular matrix (ECM) in the blastopore (7) together with the lack of effect of inhibition of ECM synthesis on blastopore initiation suggest that the mechanics of monolayers and force generation within monolayers govern blastopore formation (8, 9).

To date, research in cell mechanics has primarily focused on isolated cells, and much is now known about their mechanical properties as well as the underlying biology in normal physiology and disease (10). Comparatively little is known about the mechanics of monolayers, but recently experiments combining traction microscopy with deformation analysis have begun to shed light on this topic. Within monolayers, stresses are propagated over several cell diameters by intercellular adhesion, cells migrate to minimize intercellular shear stress (11), and the collective motion of cells within monolayers displays behaviors reminiscent of a glass transition (12, 13). Despite these advances, our knowledge of monolayer mechanical properties such as stiffness or ultimate strength remains poor due to lack of experimental techniques. Extrapolation of these parameters from single-cell measurements is not possible due to radical differences in cytoskeletal organization associated with the formation of intercellular junctions. Present measurements of intercellular adhesion energy are restricted to durations over which intercellular junctions cannot fully mature (14, 15). Direct experimental measurements on monolayers with mature intercellular junctions would greatly enhance our understanding of the mechanics of epithelial morphogenesis (16, 17) and the effect of pathologies on tissue strength (4).

We have developed a versatile, unique system that allows investigation of the tensile planar mechanical properties of epithelial cell monolayers in isolation from their substrate. We exploit these capabilities to acquire a consistent set of time-resolved quantitative measurements of monolayer mechanics at multi-, uni-, and subcellular scales and provide a detailed characterization of monolayer mechanical properties. Through the spatial organization of their cytoskeleton and interfacing via specialized intercellular adhesions, cells create a tissue that has a much higher elastic modulus than measured in single cells.

Results

Cell Monolayer Culture and Testing Device. The general principle of our system to characterize monolayer mechanics is simple: Monolayers suspended between the extremities of two test rods (one soft and one stiff) are slowly extended by prying the rods apart with a micromanipulator. The applied force can be measured by monitoring the bending of the soft test rod during mono-

Author contributions: A.R.H., A.J.K., and G.T.C. designed research; A.R.H., J.B., and B.B. performed research; A.R.H., L.P., and G.T.C. contributed new reagents/analytic tools; A.R.H. analyzed data; and A.R.H., A.J.K., and G.T.C. wrote the paper.

The authors declare no conflict of interest.

This article is a PNAS Direct Submission.

[1]To whom correspondence should be addressed. E-mail: g.charras@ucl.ac.uk.

This article contains supporting information online at www.pnas.org/lookup/suppl/doi:10.1073/pnas.1213301109/-/DCSupplemental.

layer extension (Fig. S1). Our mechanical characterization setup addresses four key requirements: (*i*) monolayers must be free from their substrate such that only the monolayer is load-bearing to allow for simple interpretation of the stress–strain response (Fig. 1), (*ii*) attachment of the samples to the test rods must require minimal manipulation, (*iii*) live microscopy imaging at the cellular and subcellular level must be possible during mechanical stimulus, and (*iv*) measurements must be quantitative to enable comparison between treatments.

To generate cell monolayers free from a substrate with minimal manipulation, we cultured cells on a temporary sacrificial substrate created by polymerizing a drop of collagen between the two rods. Cells were seeded onto this scaffold and cultured until the monolayer extended from one test rod to the other, covering the whole collagen substrate and part of each test rod (Fig. 1*A*). Prior to mechanical testing, the collagen was removed by enzymatic digestion, leaving the monolayer attached to the test rods by cell–substrate adhesion but devoid of substrate and freely suspended in between (Fig. 1*B*). In the absence of substrate, monolayers stayed healthy and maintained their characteristic epithelial apico-basal polarization for at least 3 h (Fig. 1*C* and Fig. S2).

The mechanical testing equipment (Fig. S1*A*) consisted of two micromanipulators and a top-down macroscope to image-test rod positions. A manual micromanipulator kept one rod stationary, while a motorized micromanipulator controlled the displacement of the other. To generate quantitative measurements of monolayer mechanical properties, we developed our culture system to allow for force measurements. Devices consisted of two main components (Fig. S1*B*): (*i*) a U-shaped glass capillary with one long arm that acts as a rigid reference rod and a short arm that connects to the flexible test rod, and (*ii*) a flexible test rod made of NiTi metal wire with a small enough bending rigidity for sub milli-Newton forces to induce a deflection precisely measurable by the macroscope. Forces applied onto the monolayer during extension were determined by measuring the deflection d of the wire relative to its predicted unstressed position (dotted line, Fig. S1*B*) and fitting $d(y)$ with a simple cantilevered beam model (*SI Materials and Methods* and Fig. S3).

Tissue-Level Mechanics. Using our experimental setup, we characterized the mechanical properties of monolayers of Madine–Darby Canine Kidney (MDCK-II) cells, a classic epithelial cell model. In the following, unless otherwise noted, we report the engineering strain: $\varepsilon = \Delta L/L_0$, with ΔL the monolayer length change and L_0 its original length (Fig. S4).

Living tissues are intrinsically viscoelastic with both physical and biological phenomena contributing to their time-dependent mechanical properties. Measured physiological strain rates in monolayer covered tissues range from approximately $0.04\% \cdot s^{-1}$ in developing drosophila embryos (18) and tens to hundreds of $\% \cdot s^{-1}$ in alveolar epithelium and mitral valve tissue (19, 20). To investigate the time-dependent mechanical properties of monolayers, we characterized their creep response to two distinct step increases in stress, respectively with high (3 kPa) and low stress (0.7 kPa). When the monolayers were subjected to low stress loading, strain increased rapidly in response to stress application before reaching a plateau that subsisted over 200 s (Fig. 2*A*, grey line). In contrast, when high stress loading was applied, no plateau was reached and strain increased continually with time (Fig. 2*A*, black line). Plotting these response curves in log–log scale revealed that monolayer creep followed a power law in response to high-stress step loading but not following low-stress step loading (Fig. 2*A*, inset), suggesting that monolayers behave as viscoelastic solids below a certain critical stress and as complex fluids above. Power law creep responses had an exponent $\beta = 0.15 \pm 0.03$, slightly less than generally reported for single cells [$\beta \sim 0.3$–0.5 (21)]. Consistent with the observations upon low-stress loading, stress relaxation of monolayers also reached a plateau after approximately 50 s (Fig. S5*E*), suggesting a limit for elastic behavior. Estimates of relaxation rates for computational models and comparative studies could be obtained by fitting stress relaxations with appropriate rheological models (*SI Materials and Methods* and Fig. S5 *G–H*). The time scales needed

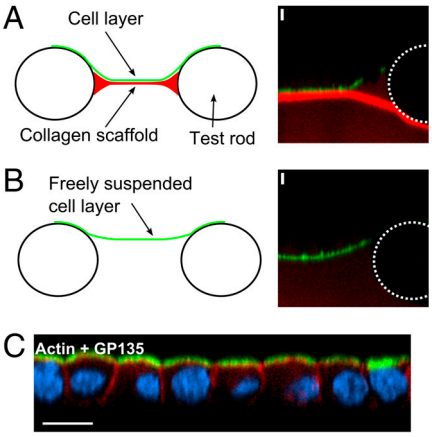

Fig. 1. Experimental setup for measuring the mechanical properties of cell monolayers. (*A*) (*Left*) Line drawing and (*Right*) microscopy image. Cell layers (green) were cultured on a sacrificial collagen scaffold gelled between the test rods (red in line drawing and immunostain, scale bar s.b = 100 μm). (*B*) After enzymatic digestion, the collagen layer was completely removed, leaving the monolayer freely suspended between the two test rods as evidenced by the loss of collagen immunostaining (red). (*C*) ZX profile of a suspended monolayer 3 h after collagen digestion. F-actin is shown in red, gp135 (a classic apical polarity marker) is shown in green, nuclei are shown in blue. Suspended monolayers retained their characteristic polarization despite removal of the substrate. (s.b = 100 μm)

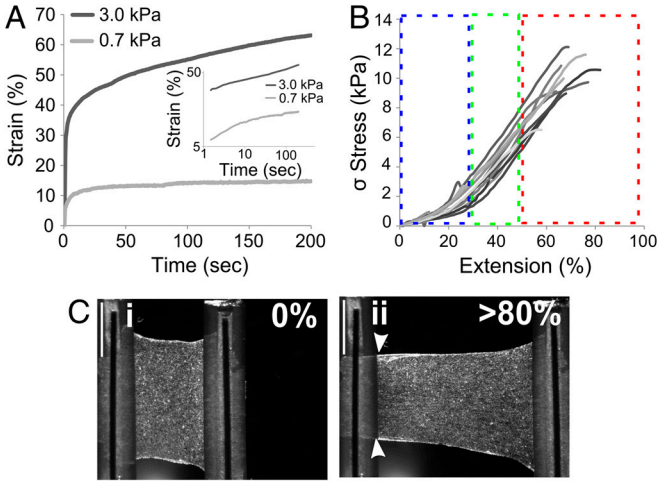

Fig. 2. Mechanical properties of cell monolayers. (*A*) Creep response following step application of low (0.7 kPa, grey) and high (3 kPa, black) stress. The plotted responses are averaged over at least six experiments each. At low stress, following a rapid increase in strain, monolayers reached a plateau that lasted for the remainder of the experiment. At high stress, no plateau was reached and strain increased continually with time. (*Inset*) Creep response curves plotted in log–log scales. The creep response at high stress (black) was well fitted by a linear function with slope $\beta = 0.15 \pm 0.03$; whereas at low stress the creep response was not linear. (*B*) Stress-extension curves shown for 12 different monolayers. All curves displayed three distinct regimes of loading: (*i*) an initial "toe" region (blue box) as the monolayer becomes loaded under tension, (*ii*) a linear extension regime (green box) from which an elastic modulus can be calculated, and (*iii*) a plateau (red box) which corresponds to plastic deformation and eventual failure. (*C*) Deformation of a monolayer under stretch. Images acquired by bright-field microscopy for a monolayer at 0 and >80% extension. At >80% extension, the monolayer delaminated from the test rods (arrows) suggesting that cell–cell adhesion is stronger than cell–substrate adhesion for this geometry. (s.b = 1 mm)

to reach a plateau in low-stress creep and stress relaxation experiments (approximately 50 s) suggest that the short time-scale response likely arises from biochemical properties of the cell, such as the turnover of the actin cytoskeleton [$t_{1/2} \sim 10$ s in MDCK cells (22)]. However, further work will be necessary to fully explore the rheological behaviors of monolayers and determine what biological mechanisms underlie their time-dependent mechanical behavior.

Next, we decided to focus on monolayer mechanical properties at strain rates between $0.5\% \cdot s^{-1}$ and $5\% \cdot s^{-1}$ that are relevant for embryonic morphogenesis where only very slow deformations take place [approximately $0.04\% \cdot s^{-1}$(18)]. To determine the elasticity and ultimate strength of monolayers, we acquired stress-extension curves until failure (Fig. 2*B* and Movie S1). For strain rates between $0.5\% \cdot s^{-1}$ and $5\% \cdot s^{-1}$, we did not observe any significant differences in measured elastic moduli, indicating that loading was quasi-static (Fig. S4*A*), and we settled on a strain rate of $1\% \cdot s^{-1}$ for our measurements. All stress-extension curves shared the following characteristic features: (*i*) a "toe" region where stress increased slowly and nonlinearly between 0 and approximately 25% extension, (*ii*) a linear region between approximately 25% and 50% extension, (*iii*) mechanical failure (for extensions >70%), following a plateau of the curve. Monolayer stiffnesses were computed from the slope of the stress–strain curves in the linear region where monolayer differential stiffness was constant (Fig. S4*B*). Measured stiffnesses averaged $E = 20 \pm 2$ kPa, two orders of magnitude larger than the elasticity of MDCK cell monolayers probed in the transversal direction by atomic force microscopy (AFM) (23). The average strain at failure was a remarkable $69 \pm 14\%$ with failure occurring by delamination, suggesting that adhesion of monolayers to the test rods was weaker than cell–cell adhesion (Fig. 2*C* and Movie S1). In cyclic loading experiments, monolayer stiffness did not vary significantly with loading cycle for small amplitudes (approximately 3%, Fig. S5*D*) but did for larger amplitudes (approximately 10–20%, Fig. S5 *C* and *D*). This suggested that MDCK monolayers underwent partial fluidization for large strain amplitudes, consistent with the existence of a threshold stress in our creep experiments and reports examining fluidization in single MDCK cells (13).

Cellular-Level Mechanics. To understand how monolayers could withstand such large strain, we analyzed deformations at the cell and tissue level. Monolayer deformations can occur through two mechanisms: shape change of the constituent cells, or reorganization of cellular arrangement within the monolayer, a process known as intercalation (24). One mechanical hallmark of intercalation is that the tissue-level strain tensor does not match the cellular-level strain tensor (18), and therefore we compared tissue strain to cell strain during extension.

We measured the tissue-level strain by computing the displacement of a grid of points within the monolayer using low magnification images (texture correlation, *SI Materials and Methods* and Fig. 3*A*). The tissue strain ε_{xx} throughout the monolayer was tightly distributed around the value of the imposed engineering strain (Fig. 3 *B* and *C*). In the transverse direction, tissue strain ε_{yy} was tightly distributed around zero (Fig. 3 *B* and *C*) but displayed a small inward contraction at the outer boundaries. Three-dimensional isosurface reconstructions of cells within the monolayer during extension revealed that the increase in projected surface area of the monolayer (Fig. 4*A*, top view, red before extension, green at 50% strain) was accompanied by thinning of the cells (Fig. 4*A*, side view) perpendicular to the monolayer plane, thereby maintaining cell volume constant (Fig. 4*B*). This indicated that the large increase in projected surface area was not accommodated by the small magnitude of the inward contraction noted at outer boundaries, but rather by preferential thinning of the monolayer in the transverse direction. This also suggested that, as expected from their cytoskeletal organization, monolayers

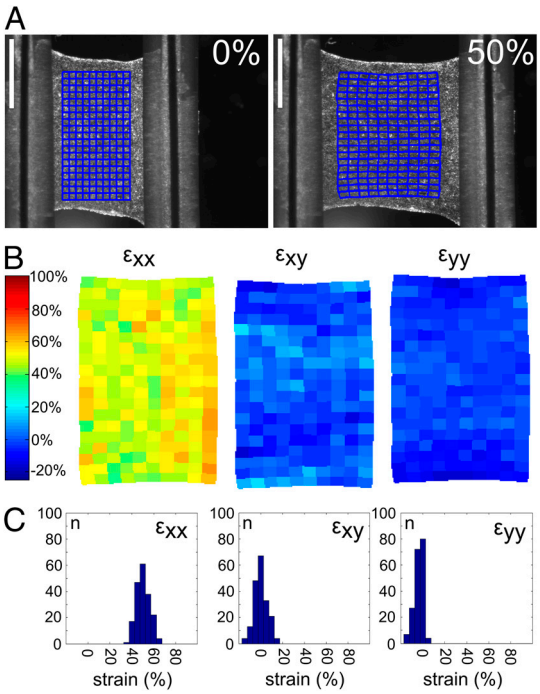

Fig. 3. Monolayer mechanics at the tissue level. (*A*) Using texture correlation, the position of nodes in the blue grid in the monolayer at rest could be tracked in the stretched monolayer. s.b = 1 mm. (*B*) This allowed computation of the strain fields ε_{xx}, ε_{xy}, and ε_{yy}. (*C*) ε_{xx} was quasi-uniform throughout the monolayer with values close to the engineering strain computed from the applied extension ($50 \pm 6\%$). ε_{yy} was also quasi-uniform throughout the sheet with average values close to zero ($-3 \pm 4\%$). Some contraction was apparent at the edges, typical for a material of this geometry. ε_{xy} was also quasi-uniform throughout the monolayer during extension ($0 \pm 6\%$). In the graphs, *n* denotes the number of grid cells that have a given strain.

have anisotropic mechanical properties. During wound healing experiments, monolayers are put under tension by the migration of leader cells at the wound edge leading to the highly heterogeneous distribution for ε_{xy} that guides collective migration of cells within the monolayer (11). In contrast, in our experiments ε_{xy} was tightly distributed around zero, presumably due to the uniform displacement applied to the monolayer and the far more rapid application of stress. The homogeneity of the strain field demonstrates that the cell properties, in particular their stiffnesses, are uniform across the monolayer. The absence in suspended epithelia of the typical patterns of cell displacements visible on dense epithelia migrating on a substrate (11) confirmed the requirement for strong cell–substrate interactions in the emergence of collective migration patterns.

Cellular-level strain was characterized by measuring changes in cellular long-axis length and orientation from segmented images of monolayers expressing E-cadherin GFP (Fig. 4 *C*–*E*, Fig. S6, and *SI Materials and Methods*) (18). During extension, the cellular-level strain matched tissue-level strain, suggesting that no intercalation took place (Fig. 4*F*). Average long-axis orientation changed from having a small level of orientation anisotropy at rest, possibly due to small magnitude stresses arising after substrate removal, to displaying a much stronger anisotropy when the sheet was stretched (Fig. 4*G*). Together these data show that cultured monolayers extend solely due to shape change of their cellular components with no intercalation. Consistent with these mechanical measurements, on the time scales of the experiments (approximately 5 min), microscopy examination of the cells did not reveal cell rearrangement or division.

Subcellular Mechanics: Cytoskeletal Deformation During Extension. The cytoskeleton plays a major role in single cell mechanical

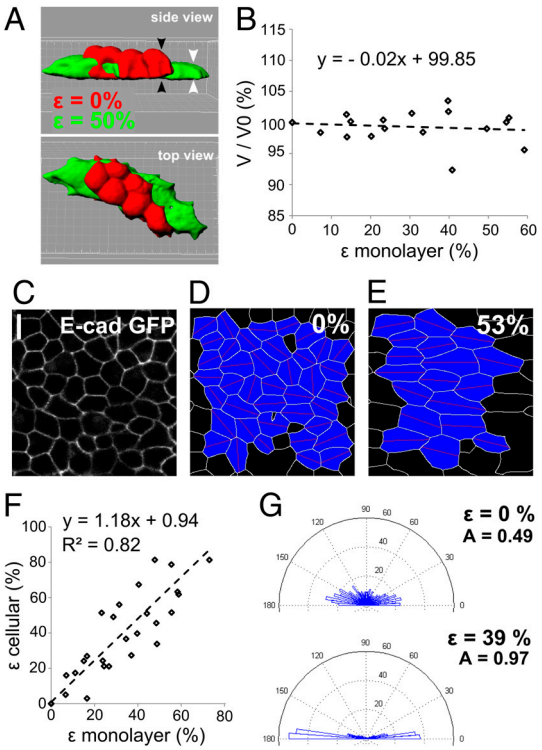

Fig. 4. Monolayer mechanics at the cellular level. (*A*) Three-dimensional isosurface reconstruction of cells within a monolayer before (red) and after (green) extension. Cell height decreased with extension (side view: black arrowheads: 0% strain, white arrowheads: 50% strain) but cellular projected area increased (top view). (*B*) Cell volume was conserved during extension, suggesting that the constituent cells are incompressible. (*C–E*) Segmented images of cells expressing E-cadherin GFP were used to calculate the cellular deformations before and during stretch. (*F*) The calculated cellular strain matched the monolayer strain near perfectly, indicating that no intercalation takes place during extension. (*G*) The orientation of cell-long axes prior to stretch was widely distributed with a small bias along the *x*-axis but, during stretch, cellular orientations were nearly exclusively aligned with the direction of extension. The anisotropy of alignment calculated as $A = 1 - (\%\text{alignedperpendicular})/(\%\text{alignedparallel})$ almost doubled when the cells were subjected to 39% strain.

properties and, in tissues, loss of function mutations affecting cytoskeletal and adhesive proteins lead to increased fragility. We examined cytoskeletal organization during monolayer extension paying particular attention to protein constituents of adherens junctions and desmosomes, key structures in intercellular junctions.

In adherens junctions, adjacent cell membranes are tethered to one another by classical cadherins (E-cadherin in epithelial cells) that are linked intracellularly to the actomyosin cytoskeleton, thus integrating neighboring cells into a mechanical syncytium (25). Removal of the collagen substrate led to a general rounding of the cells and a reduction in projected surface area due to loss of basal adhesion (Fig. 5 *A* and *B* and Fig. S4) but no change in the localization of E-cadherin was observed. E-cadherin distribution was not affected by extension (Fig. 5 *B* and *C*). F-actin remained localized to intercellular junctions (Fig. 5 *D* and *E*) but had a somewhat less uniform distribution under strain displaying some enrichment at tricellular junctions (Fig. 5*F*). Myosin regulatory light chain (MRLC), a component of myosin II whose phosphorylation controls contractility, displayed a dramatic change in localization upon removal of the substrate and under strain. Localization changed from being cytoplasmic (Fig. 5*G*) to punctate and junctional (Fig. 5 *H* and *I*), reminiscent of myosin localization in embryonic epithelial tissues (5) and suggesting a role for myosin contractility in monolayer mechanics.

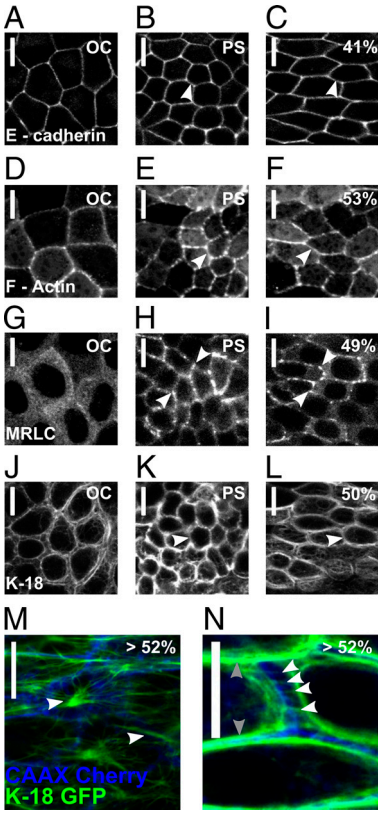

Fig. 5. Subcellular organization in stretched monolayers. OC: On collagen, PS: pre-stretch, % indicates the percentage strain (s.b = 10 μm). (*A–C*) E-cadherin GFP remained localized to cell junctions in all conditions. (*D–F*) Life-act GFP, an F-actin marker, remained localized at cell junctions throughout extension but appeared less uniform at low stretch. (*G–I*) The regulatory light chain of myosin was primarily cytoplasmic in cells on collagen (*G*), but underwent a dramatic relocalization to cell junctions pre-stretch (*H*) and at high extension (*I*). (*J–L*) The keratin 18 filament network spanned the entire monolayer on collagen (*J*) and looked largely bundled prior to extension (*K*). Application of stretch induced rearrangement of the filaments, suggesting that they served to transmit stress across cell boundaries (arrowhead). (*M*) Keratin filaments (green) formed an intercellular network with nodes at the cell centres (white arrows) that linked cells to one another across cell boundaries (blue) in stretched monolayers. (*N*) Keratin filaments (green) appeared tensed across cell junctions (blue) perpendicular to the direction of extension (white arrows) and bundled (grey arrows) at cell junctions parallel to the direction of extension.

Desmosomes link the keratin intermediate filaments of neighboring cells to one another, forming a second supracellular cytoskeletal network. Genetic mutations of keratins or desmosomal proteins result in fragile epithelia (4). On collagen, keratin localized perinuclearly with short wavy segments linking cells to one another (Fig. 5*J*). After removal of collagen, keratin filaments remained perinuclear (Fig. 5*K*), and at high strain, filaments became aligned in the direction of stretch (Fig. 5*L*). When imaged at higher magnification, a keratin supracellular network was clearly visible (Fig. 5*M*) and filaments straddling intercellular junctions appeared taut and aligned parallel to the direction of extension (Fig. 5*N*, arrows). This change in conformation from wavy at low strain to taut at high strain suggested that keratins are involved in a nonlinear mechanical response of the monolayer to stretch, as proposed by others (26, 27) and consistent with the mechanical properties of isolated keratins and keratin networks in cells(27, 28).

Subcellular Perturbations Lead to Changes in Tissue-Level Mechanics. We examined how perturbations at the molecular scale affected mechanics at the tissue scale. The filamentous actin network is a

key contributor to cellular elasticity in isolated cells and, in monolayers, it is the main component of adherens junctions. When we depolymerized the actin cytoskeleton of monolayers with latrunculin B, their stiffness decreased by approximately 50% compared to controls ($E_{\text{latrunculin}} = 10 \pm 6$ kPa, $p < 0.01$, Fig. 6*A* and *B*), demonstrating the importance of F-actin for monolayer stiffness. Next, we asked if myosin contractility contributed to monolayer mechanics based on its localization to intercellular junctions (Fig. 5*I*). Treatment of monolayers with Y27632, an inhibitor of rho-kinase mediated contractility, led to a significant approximately 36% decrease in stiffness ($E_{Y27632} = 13 \pm 6$ kPa, $p < 0.01$). Hence, myosin contractility contributes to monolayer elasticity. Ultimate strain did not change with treatments affecting F-actin or contractility (Fig. 6*C*).

Intercellular Adhesion in Monolayers. During ultimate strength measurements, control monolayers normally failed by delamination from the test rods, suggesting that failure occurred through rupture of cell–substrate adhesions (Movie S1 and Fig. 2*C*). To induce failure through rupture of intercellular adhesions, we concentrated stresses by narrowing tissue width by nicking the unstressed sheet prior to extension. Under these conditions, failure occurred at local strains of $110 \pm 18\%$, more than doubling monolayer length. Cracks initiated in the monolayer close to the nicked region and propagated perpendicularly to the direction of stretch across the sheet width (Fig. 6 *E*–*G* and Movie S2). Knowing the monolayer elasticity ($E = 20$ kPa) and choosing the cell diameter $a \sim 10$ μm as a natural length scale within the monolayer, we could estimate the intercellular adhesion energy density per unit area Γ within the monolayer: $\Gamma = a\sigma^2/2E = 0.07$ N.m^{-1} with $\sigma = 17 \pm 3$ kPa the ultimate stress (Fig. S7). The average force required to separate two cells within the monolayer is $F_{\text{doublet}} \sim F_{\text{total}}/N \sim 1.7$ μN with $F_{\text{total}} \sim 202$ μN the applied force onto the monolayer at rupture and $N \sim 120$ the average number of cells in the narrowed monolayer width. Experiments on cell doublets brought into contact for about 30 min yield a separation force $F \sim 200$ nN (14), almost nine times lower than in monolayers, perhaps reflecting the less mature intercellular junctions formed during the shorter intercellular contact time.

To verify the well-known importance of intercellular adhesion for monolayer mechanics, we disrupted cell–cell adhesion by treatment with EDTA, a divalent cation chelator that blocks cadherin-mediated adhesion. Monolayers treated with EDTA still retained sufficient integrity to withstand a small strain (<20%), but at moderate strain (approximately 25%), cracks formed within the monolayer propagating perpendicularly to the direction of stretch (Fig. 6 *H* and *I* and Movie S3). Monolayers had significantly reduced stiffnesses and intercellular adhesion energy densities compared to controls ($E = 0.8 \pm 0.4$ kPa and $\Gamma = 8.10^{-5}$ N.m^{-1}, $p < 0.01$ in both cases) (Fig. 6*D*), quantitatively confirming the well-studied role of cadherin-mediated intercellular adhesion in monolayer integrity.

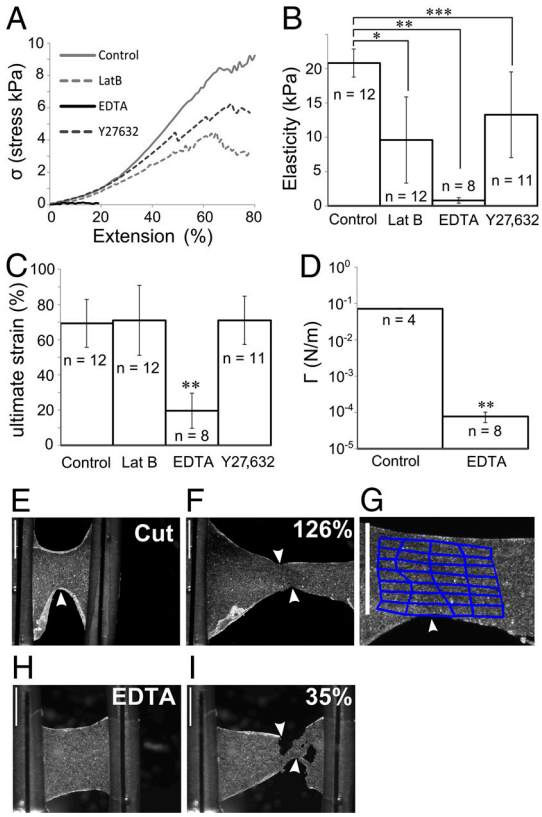

Fig. 6. The actin cytoskeleton and intercellular adhesion contribute strongly to monolayer mechanics. (*A*) Average loading curves for monolayers treated with Latrunculin B (dashed light grey line), Y27632 (dashed dark grey line), and EDTA (black line) compared to control monolayers (light grey line). (*B*) Monolayer stiffness was significantly reduced by treatment with latrunculin B, Y27632, or EDTA ($N_{\text{control}} = 12$, $N_{\text{latrunculin}} = 12^{*}$, $N_{\text{EDTA}} = 8^{**}$, $N_{Y27632} = 11^{***}$, $p < 0.01$ for all measurements). (*C*) Ultimate strength was not significantly reduced by treatment with latrunculin B or Y27632 but was significantly reduced by treatment with EDTA (**). (*D*) EDTA-treated monolayers showed a considerable reduction in their adhesion energy density ($p < 0.01^{**}$). (*E* and *F*) To induce failure through intercellular adhesion rupture in control monolayers, a nick was made in the sheet to concentrate stresses (white arrow). Monolayers failed at high strain by crack formation (*F* and *G*, 126% strain, arrows). Cracks within the monolayer formed in the region of highest local tissue strain (arrows). With EDTA treatment (*H* and *I*), cracks formed within the monolayer and propagated perpendicularly to the direction of extension (white arrows). (s.b = 1 mm)

Discussion

Using a unique culture system, we give the first detailed characterization of monolayer mechanical properties at the tissue, cellular, and subcellular scales. Live imaging during mechanical testing allowed us to relate cellular and subcellular level phenomena to tissue level mechanics. We have shown that on short time scales, extension of monolayers results solely from deformation of their constituent cells rather than intercalation and that monolayers could withstand more than a doubling in length before failure through rupture of intercellular junctions. Monolayer stiffness was two orders of magnitude larger than the elasticity of their constituent cells measured in the transversal direction by AFM (23) in monolayers grown on glass substrates, pointing to a large anisotropy in monolayer mechanical properties. The actin cytoskeleton accounted for half of the stiffness of monolayers, presumably due to its importance in forming intercellular junctions. A closer inspection of the time-dependent behavior also revealed that monolayers display complex time-dependent rheological properties. As in single cells (13), application of high amplitude cyclical strain loading led to partial fluidization of the monolayers, but the exact biological mechanisms underlying this behavior remain unknown. Consistent with experiments in embryos and isolated cells (5, 10), myosin contractility contributed significantly to monolayer mechanics, as suggested by localization of MRLC to intercellular junctions. Within monolayers, the average force required to separate two cells was approximately 1.7 μN, about ninefold larger than measured in pairs of isolated cells (14), perhaps due to the more natural configuration of the cells or the fuller maturation of intercellular junctions. Based on these measurements and the contribution of actin to the monolayer stiffness, at fracture the actin network in each individual cell bears approximately 840 nN, comparable to the maximal line tensions of approximately 400 nN borne by stress fibers (29). As expected, disruption of cell–cell adhesion led to a dramatic fragilization of cell sheets. Taken together, these data

paint a picture of monolayer mechanics where cells adhere strongly to one another and therefore can pull strongly on one another through myosin contractility, leading to the development of a tissue-level tension and as a result higher stiffness. Furthermore, such a process may be self-reinforcing with higher tensions leading to myosin recruitment (30) and increased myosin duty ratio (31). Imaging of intermediate filaments revealed that their aspect changed from wavy to taut with increasing monolayer extension, suggesting that at high strains they become load-bearing and therefore may be involved in a nonlinear mechanical response of the monolayer as previously proposed (26, 27). Such an interpretation would be consistent with the fragile epithelium symptoms observed in patients with mutations in keratins or desmosomal proteins (4) but will necessitate further study. Together our experimental methods pave the way for quantitative investigations of monolayer mechanics at the subcellular, cellular, and tissue level and they should be widely applicable to any cell type forming strong intercellular junctions.

During development, embryonic morphogenesis is in large part due to changes in the organization and mechanics of epithelial monolayers. Over the past decade, researchers have devised many experimental and computational techniques to study the mechanics of morphogenetic events, but a detailed understanding has been hindered by a lack of tools to directly characterize monolayer mechanics. For example, measurements of embryonic epithelial tension by laser cutting rely on monitoring tissue recoil, something that depends both on monolayer tension and stiffness. Though laser cutting successfully allows for comparative measurements of tension to be effected, combining it with our techniques would allow for deconvolution of tension and stiffness and hence absolute measurements. In computational models of epithelia, the contribution of cytoskeletal components (in particular actomyosin contractility) to monolayer mechanics is often accounted for by spring networks and line tensions acting in bulk or at intercellular junctions (16, 17). However, estimating the value of the corresponding parameters has proven challenging. Based on our measurements of monolayer stiffness for a range of biological and chemical perturbations, suitable estimates of these parameters can be obtained. Direct experimental measurements of monolayer mechanics combined with computational models will therefore allow for a better understanding of multicellular aggregate mechanics.

Materials and Methods

Additional information can be found in the *SI Text*.

Force Measurement Device Fabrication. Borosilicate capillaries were bent into a "U" shape and cut to size. One arm was left long to act as a rigid reference rod and the other cut short to serve as a connection for the flexible test rod (Fig. S1*B*). NiTi alloy wire was cut to length, dipped into UV-curing glue and threaded into the static rod. Another wire of similar length made up the flexible rod. Two pieces of Tygon tubing were attached to each wire to act as a substrate for collagen polymerization and cell culture. The test rods were glued to the bottom of 50-mm plastic-bottomed Petri dishes.

Cell Culture on Devices. Collagen type 1A was reconstituted on ice and a droplet was deposited between the device test rods. Devices were placed at 37 °C for 90–120 min and allowed to dry, giving a thin layer of collagen between the test rods. The collagen support was rehydrated by depositing a 10 μl droplet of culture medium on it. Approximately 25,000 cells were placed onto the collagen support and incubated at 37 °C for 30 min. Finally, culture medium was added such that the test rods were completely submerged.

ACKNOWLEDGMENTS. The authors thank Karl Matter (University College London) for generous help with antibodies and reagents and Alpha Yap (University of Queensland) for critical reading of the manuscript. We thank Duncan Farquharson and his team at the University College London Biosciences Mechanical Workshop for technical assistance. The authors acknowledge the University College London Comprehensive Biomedical Research Centre for generous funding of microscopy equipment. This work was supported by a Royal Society Equipment Grant and a Royal Society University Fellowship (to G.T.C.). A.R.H. is part of the University College London Engineering and Physical Sciences Research Council Engineering Doctorate Program.

1. Ethier CR, Simmons CA (2007) *Introductory Biomechanics: From Cells to Organisms* (Cambridge Univ Press, Cambridge, UK).
2. Fung Y-C (1993) *Biomechanics: Mechanical Properties of Living Tissues* (Springer, New York).
3. Berne RM, Levy MN (2000) *Principles of Physiology* (Mosby, Missouri, MO), 3rd Ed.
4. Getsios S, Huen AC, Green KJ (2004) Working out the strength and flexibility of desmosomes. *Nat Rev Mol Cell Biol* 5:271–281.
5. Rauzi M, Verant P, Lecuit T, Lenne P-F (2008) Nature and anisotropy of cortical forces orienting Drosophila tissue morphogenesis. *Nat Cell Biol* 10:1401–1410.
6. Levine E, Lee CH, Kintner C, Gumbiner BM (1994) Selective disruption of E-cadherin function in early Xenopus embryos by a dominant negative mutant. *Development* 120:901–909.
7. Davidson LA, Keller R, DeSimone DW (2004) Assembly and remodeling of the fibrillar fibronectin extracellular matrix during gastrulation and neurulation in *Xenopus laevis*. *Dev Dyn* 231:888–895.
8. Davidson LA, Marsden M, Keller R, Desimone DW (2006) Integrin alpha5beta1 and fibronectin regulate polarized cell protrusions required for Xenopus convergence and extension. *Curr Biol* 16:833–844.
9. Georges-Labouesse EN, George EL, Rayburn H, Hynes RO (1996) Mesodermal development in mouse embryos mutant for fibronectin. *Dev Dyn* 207:145–156.
10. Fletcher DA, Mullins RD (2010) Cell mechanics and the cytoskeleton. *Nature* 463:485–492.
11. Tambe DT, et al. (2011) Collective cell guidance by cooperative intercellular forces. *Nat Mater* 10:469–475.
12. Angelini TE, et al. (2011) Glass-like dynamics of collective cell migration. *Proc Natl Acad Sci USA*, 10.1073/pnas.1010059108.
13. Trepat X, et al. (2007) Universal physical responses to stretch in the living cell. *Nature* 447:592–595.
14. Chu Y-S, et al. (2004) Force measurements in E-cadherin—Mediated cell doublets reveal rapid adhesion strengthened by actin cytoskeleton remodeling through Rac and Cdc42. *J Cell Biol* 167:1183–1194.
15. Hobbs RP, Green KJ (2011) Desmoplakin regulates desmosome hyperadhesion. *J Invest Dermatol*, 10.1038/jid.2011.318.
16. Farhadifar R, Röper J-C, Aigouy B, Eaton S, Jülicher F (2007) The influence of cell mechanics, cell–cell interactions, and proliferation on epithelial packing. *Curr Biol* 17:2095–2104.
17. Chen HH, Brodland GW (2000) Cell-level finite element studies of viscous cells in planar aggregates. *J Biomech Eng* 122:394–401.
18. Blanchard GB, et al. (2009) Tissue tectonics: Morphogenetic strain rates, cell shape change, and intercalation. *Nat Methods* 6:458–464.
19. Perlman CE, Bhattacharya J (2007) Alveolar expansion imaged by optical sectioning microscopy. *J Appl Physiol* 103:1037–1044.
20. Sacks MS, et al. (2002) Surface strains in the anterior leaflet of the functioning mitral valve. *Ann Biomed Eng* 30:1281–1290.
21. Kollmannsberger P, Fabry B (2011) Linear and nonlinear rheology of living cells. *Annu Rev Mater Res* 41:75–97.
22. Yamada S, Pokutta S, Drees F, Weis WI, Nelson WJ (2005) Deconstructing the Cadherin-Catenin-Actin Complex. *Cell* 123:889–901.
23. Harris AR, Charras GT (2011) Experimental validation of atomic force microscopy-based cell elasticity measurements. *Nanotechnology* 22:345102–345102.
24. Wolpert L (2001) *Principles of Development* (Oxford Univ Press, Oxford, UK), 2nd Ed.
25. Gumbiner BM (2005) Regulation of cadherin-mediated adhesion in morphogenesis. *Nat Rev Mol Cell Biol* 6:622–634.
26. Ingber DE (2003) Tensegrity I: Cell structure and hierarchical systems biology. *J Cell Sci* 116:1157–1173.
27. Herrmann H, Bar H, Kreplak L, Strelkov SV, Aebi U (2007) Intermediate filaments: From cell architecture to nanomechanics. *Nat Rev Mol Cell Biol* 8:562–573.
28. Sivaramakrishnan S, DeGiulio JV, Lorand L, Goldman RD, Ridge KM (2008) Micromechanical properties of keratin intermediate filament networks. *Proc Natl Acad Sci USA* 105(3):889–894.
29. Deguchi S, Ohashi T, Sato M (2006) Tensile properties of single stress fibers isolated from cultured vascular smooth muscle cells. *J Biomech* 39:2603–2610.
30. Fernandez-Gonzalez R, Simoes SdM, Röper J-C, Eaton S, Zallen JA (2009) Myosin II dynamics are regulated by tension in intercalating cells. *Dev Cell* 17:736–743.
31. Ren Y, et al. (2009) Mechanosensing through cooperative interactions between myosin II and the actin crosslinker cortexillin I. *Curr Biol* 19:1421–1428.